Angle-resolved photoemission study of the submonolayer phases of Pb on Ge(111)

J. A. Carlisle, T. Miller, and T.-C. Chiang
Department of Physics, University of Illinois at Urbana-Champaign, 1110 West Green Street, Urbana, Illinois 61801
and Materials Research Laboratory, University of Illinois at Urbana-Champaign, 104 South Goodwin Avenue, Urbana, Illinois 61801
(Received 28 October 1992)

The $(\sqrt{3}\times\sqrt{3})R30°$ α and γ submonolayer reconstructions of the Pb/Ge(111) system have been studied with angle-resolved photoemission spectroscopy utilizing synchrotron radiation. The α phase consists of $\frac{1}{3}$ monolayer (ML) of Pb adatoms in T_4 sites, whereas the γ phase consists of an equal mix of Pb ($\frac{1}{6}$ ML) and Ge ($\frac{1}{6}$ ML) adatoms, forming a mosaic phase. Dispersions of the adatom-induced surface states of the γ and α phases have been probed along the $\overline{\Gamma M}$ and $\overline{\Gamma KM}$ directions of the surface Brillouin zone. Our results indicate that despite their structural differences, the α and γ phases have essentially the same electronic structure. Comparisons are made between this system and prototypical metal/Si(111)-$(\sqrt{3}\times\sqrt{3})R30°$ systems and with theory.

I. INTRODUCTION

Much effort has been made in recent years towards an understanding of the geometric structure of clean and adsorbate-covered semiconductor surfaces. Several studies have succeeded in explaining the connection between the adsorbate bonding geometry relative to the substrate and the measured surface band structure as probed by angle-resolved photoemission. The most notable successes are the Si(111)-$(\sqrt{3}\times\sqrt{3})R30°$ reconstructions induced by various group-III and group-IV adatoms: Ga,[1] In,[1,2] Al,[3-5] and Sn,[1] as well as the Si(111)-(7×7) surface.[4,6,7] In comparison, little angle-resolved photoemission work has been published on metal/Ge(111) adsorbate systems.[8]

Pb overlayers on Si and Ge substrates have received some attention recently. Since Pb is insoluble in Si and Ge, the complications arising from intermixing of the adsorbate and substrate atoms are eliminated.[9] Consequently, the Pb/Si(111) and Pb/Ge(111) systems have been probed with numerous techniques, including our own detailed core-level and angle-integrated valence-band studies.[10,11] An intriguing characteristic of both of these systems is that each has two different $(\sqrt{3}\times\sqrt{3})R30°$ reconstructions in the submonolayer regime. In addition to the expected $\frac{1}{3}$ monolayer (ML) phase (labeled the α phase), each displays a "mosaic" $(\sqrt{3}\times\sqrt{3})R30°$ reconstruction, whose ideal Pb coverage is $\frac{1}{6}$ ML. This reconstruction will be referred to as the γ phase. A mosaic phase has also been observed for the Sn/Si(111) system.[12] Based on our previous photoemission studies as well a scanning-tunneling-microscope (STM) study,[13] these mosaic γ phases consist of an equal number of Pb and Ge (or Si) adatoms on the surface, each occupying so-called T_4 sites. A natural question arises as to the electronic structure each of these different types of adatoms may give rise to when Pb and Ge (Si) adatoms are present on the surface simultaneously. Do the differing dangling bonds and back bonds yield distinctly different surface bands, or do they result in shifts of the bands found in the α phase? The purpose of the current study is to probe these differences in electronic structure with angle-resolved photoemission.

II. EXPERIMENTAL DETAILS

The photoemission experiments were performed at the 1-GeV storage ring Aladdin at the Synchrotron Radiation center of the University of Wisconsin–Madison. A small hemispherical analyzer mounted on a two-axis goniometer was employed to detect electrons emitted from the sample with an angular resolution of about ±1.5°. All binding energies were measured relative to the Fermi level, which was taken from a gold foil in electrical contact with the sample. The photon energy used to acquire all angle-resolved data was 20 eV, and the angle which the incoming photon beam made with the sample normal was kept at 45°. All spectra were acquired with the sample at or near room temperature. The Ge(111) sample used was oriented with the Laue technique and polished to a mirror finish. The sample was then chemically etched prior to chamber insertion. Final preparation of the Ge(111) surface was accomplished by multiple cycles of Ar^+ ion bombardment at ~500 °C, followed by a 15-min anneal at 800 °C. This procedure consistently yields very sharp $c(2\times8)$ reflection high-energy electron-diffraction patterns along with strongly pronounced surface core levels and surface states. High-purity (99.999%) Pb was evaporated from a tungsten crucible heated with a feedback-controlled electron beam. The deposition rate was determined using a quartz-crystal thickness monitor. The coverage units used refer to the unreconstructed Ge(111) substrate: 1 ML≡7.21 $\times10^{14}$ atoms/cm^2=one-half of a Ge(111) double layer.

III. RESULTS

The γ and α phases were prepared by depositing $\frac{1}{6}$ or $\frac{1}{3}$ ML of Pb, respectively, onto a clean Ge(111)-$c(2\times8)$ substrate held at a constant temperature of 200 °C. Al-

though these phases will form on a Ge(111) surface at room temperature, our previous study revealed that the long-range order of the reconstructions could be significantly improved by deposition at elevated temperatures, or by postdeposition annealing.[11] Note that the annealing temperature of 200 °C is far below the desorption temperature of Pb (~350 °C), so that the amount of Pb on the surface is unaffected by the annealing. Ge 3*d* and Pb 5*d* core levels as well as angle-integrated valence-band spectra were checked after deposition and annealing to confirm that the surfaces were of similar quality to those studied by us previously.[11]

Figure 1 shows the real-space and corresponding reciprocal-space diagrams appropriate to the $(\sqrt{3}\times\sqrt{3})R30°$ reconstructions. The $(\sqrt{3}\times\sqrt{3})R30°$ and (1×1) unit cells are shown as solid and dashed lines, respectively. Pb atoms in the α phase occupy the so-called T_4 sites, which are threefold-coordinated sites situated directly above Ge atoms in the lower half of the first double layer. These T_4 sites have been shown to result in a lower free energy as compared to the H_3 sites, which are also threefold sites but lie above Ge atoms in the second double layer.[5,6] Angle-resolved valence-band spectra were acquired along the principal symmetry directions in the $(\sqrt{3}\times\sqrt{3})R30°$ surface Brillouin zone (Fig. 1). Note that the symmetry of the reconstruction eliminates complications that arise in multiple-domain reconstructed surfaces, such as the clean Ge(111)-$c(2\times8)$ surface. The directions probed were the $[1\bar{1}0]$ and $[\bar{1}2\bar{1}]$ bulk directions, which correspond to the $\bar{\Gamma}\bar{M}$ and $\bar{\Gamma}\bar{K}\bar{M}$ axes, respectively.

Figures 2–5 show the angle-resolved photoemission data. In each of these figures the spectra are shown in stack-plot form for increasing electron emission angles θ. Normal emission corresponds to $\theta=0°$. The parallel momentum of the photoelectrons, $\mathbf{k}_{\parallel}$, *increases* upwards in each figure, and *decreases* as the binding energy increases at a given emission angle. The labels $\bar{\Gamma}$, $\bar{K}$, and $\bar{M}$ in each figure denote the (approximate) zone boundaries of the $(\sqrt{3}\times\sqrt{3})R30°$ surface Brillouin zone. In all of these figures surface states are clearly observed, which move in binding energy as the electron emission angle (parallel momentum) is changed. Many bulk features were also detected in the 10–2.5-eV binding-energy range (not shown in Figs. 2–5); the dispersion of the bulk bands has been mapped out in other work.[8,14]

Figure 2 shows four separate and distinct surface-state features along the $\bar{\Gamma}\bar{K}\bar{M}$ direction for the α phase. These

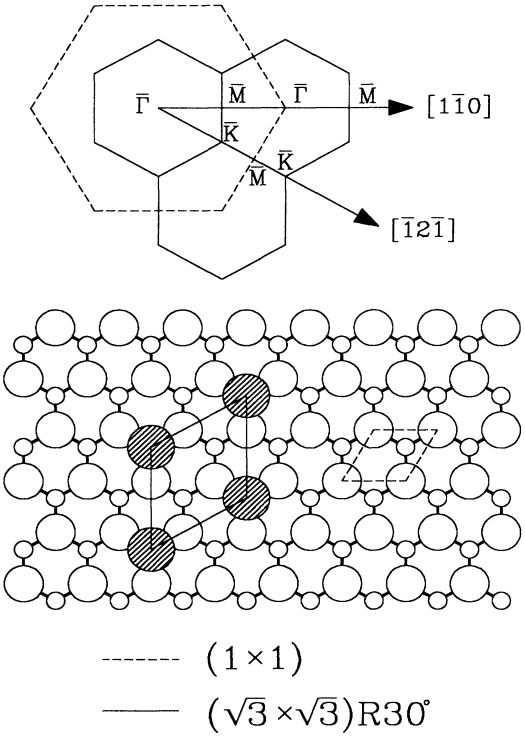

FIG. 1. The real-space and reciprocal-space diagrams appropriate for the Pb/Ge(111)-$(\sqrt{3}\times\sqrt{3})R30°$ system under study. Large and small open circles depict the first double layer of Ge atoms present at the (111) surface. The larger hatched circles show the Pb atoms arranged in a $(\sqrt{3}\times\sqrt{3})R30°$ T_4 adatom geometry. The solid and dashed lines denote the $(\sqrt{3}\times\sqrt{3})R30°$ and (1×1) unit cells, for both the real- and reciprocal-space diagrams. The symmetry points in reciprocal space are indicated.

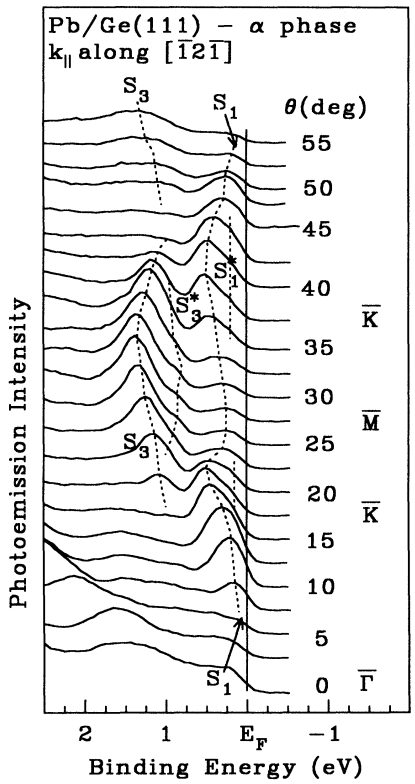

FIG. 2. Photoemission spectra acquired from the α phase along the $\bar{\Gamma}\bar{K}\bar{M}$, or $[\bar{1}2\bar{1}]$, direction. The photon energy used was 20 eV. Emission angle θ increases upwards in the figure. The binding energy is with respect to the Fermi level. The dashed lines indicate surface-state features.

are labeled S_1, S_1^*, S_3, and S_3^*. State S_1 is observable for emission angles $7.5° \leq \theta \leq 20°$ and $35° \leq \theta \leq 52.5°$, whereas the weak shoulder feature S_1^* is visible at emission angles around 17.5° and 40°. States S_3 and S_3^* are prominent for emission angles $17.5° \leq \theta \leq 37.5°$. The S_3 state is also visible at large emission angles $>45°$. The broad feature first visible for $\theta = 0°$ at binding energy $E_b = 1.5$ eV is due to emission from bulk bands, as has been observed previously.[8,14] S_1 is first visible at a binding energy of 0.15 eV, and disperses upward to a maximum value of $E_b = 0.50$ eV. S_1^* has a nearly constant binding energy of ~ 0.15 eV. The S_3 feature has minimum and maximum binding energies of 1.08 and 1.35 eV, respectively, whereas S_3^* ranges from 0.85 to about 1.00 eV. The bandwidths of the S_1, S_3, and S_3^* bands are thus approximately 0.35, 0.27, and 0.15 eV, respectively.

Figure 3 displays the data for $\overline{\Gamma KM}$ direction collected from the γ phase. As discussed in the Introduction, this surface has the same periodicity and basic surface structure as the α phase, but with half of the Pb adatoms replaced with Ge adatoms. As can be seen in Fig. 3, in addition to the surface bands present in the α phase, one new feature, labeled S_2, is visible for a narrow emission range $2.5° \leq \theta \leq 17.5°$ with E_b ranging from 0.70 to 0.85 eV. The state S_1^* is again observed but over a somewhat wider emission range, and appears slightly better defined as compared to the α phase. The intensity of the S_1 band is reduced for the γ phase, as compared to its intensity on the α phase. The intensity of the S_3 band appears to be roughly the same for the two phases. The S_3^* band is not as well defined on the γ surface as compared to the α surface.

The angle-resolved photoemission spectra acquired for the α phase along the $\overline{\Gamma M}$ direction are shown in Fig. 4, where again the dispersion of four separate features S_1, S_1^*, S_3, and S_3^*, are clearly visible. The S_1 surface state is visible for emission angles $7.5° \leq \theta \leq 25°$ and $45° \leq \theta \leq 62.5°$, with binding energies ranging from 0.15 to 0.35 eV. The state labeled S_1^* appears at 35° at a binding energy of ~ 0.5 eV. The S_3 and S_3^* features are also visible over a wide range in momentum space, but the mapping of these features is ambiguous in light of the spectra obtained at emission angles around $\theta = 50°$. At this angle there appear to be at least four bumps detected. The S_3 surface state is first visible at $\theta = 15°$ at a binding energy of ~ 1.0 eV. It disperses upward to a value of 1.65 eV, yielding an overall bandwidth of 0.65 eV. S_3^* appears for emission angles $15° \leq \theta \leq 22.5°$ and $50° \leq \theta \leq 65°$, with binding energies ranging from 1.35 to 0.83 eV. The bandwidth of this surface state is thus approximately 0.52 eV.

Figure 5 displays spectra obtained from the γ phase along the $\overline{\Gamma M}$ direction. Once again, in addition to the S_1, S_1^*, S_3, and S_3^* states, the feature labeled S_2 is observed. The S_2 state is visible only over a small range of angles, $2.5° \leq \theta \leq 7.5°$, with binding energies from 0.65 to

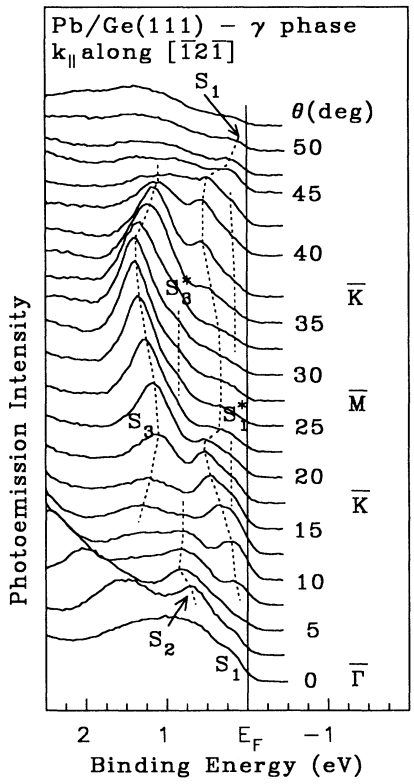

FIG. 3. Same as Fig. 2, but for the γ phase.

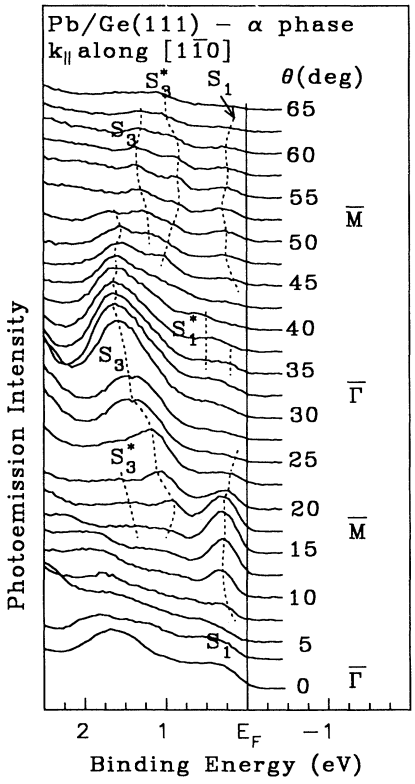

FIG. 4. Same as in Fig. 2, but now the emission angle is varied along the $\overline{\Gamma M}$, or $[1\bar{1}0]$, direction.

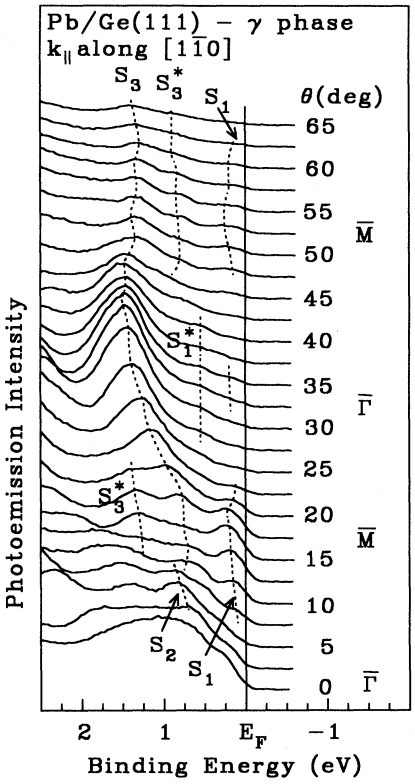

FIG. 5. Same as in Fig. 4, but for the γ phase.

0.80 eV. As opposed to the α phase, emission at $\theta = 50°$ and nearby angles appears to be less ambiguous for the γ phase. As was seen before along the $[\bar{1}2\bar{1}]$ direction, the S_1 intensity appears to be reduced for the γ phase in comparison to the α phase. The intensity of the S_3 state again appears unchanged. The other major difference between the α and γ phases in the $\bar{\Gamma}\bar{M}$ direction is the binding-energy position of the S_3 band. For the γ phase, the position of this band is shifted about 0.15 eV to higher binding energy for emission angles $\geq 30°$.

IV. DISCUSSION

In Figs. 6 and 7 the energy dispersions of the surface states detected along the $\bar{\Gamma}\bar{K}\bar{M}$ and $\bar{\Gamma}\bar{M}$ directions, for both the α and γ phases, are plotted versus the parallel momentum of the photoelectrons, $\mathbf{k}_{\parallel}$, in units of Å^{-1}.[15] Figure 6 (7) represents the data shown in Figs. 2 and 3 (4 and 5). Some additional data (angles), which are not shown in Figs. 2–5, also appear in these figures. In each of these figures, the solid symbols indicate strong features whereas the weak features are denoted by open symbols. Circles correspond to surface states detected for the α phase; triangles denote those observed on the γ surface. The solid vertical lines denote high-symmetry points of the $(\sqrt{3}\times\sqrt{3})R30°$ unit cell (see Fig. 1).

Upon inspection of Figs. 6 and 7, it is immediately apparent that the electronic structure of the γ and α surfaces is essentially equivalent. The main differences are (a) the presence of the S_2 state for the γ phase, (b) the S_3 states differ in binding energy by about 0.15 eV near the second $\bar{\Gamma}$ point along the $[1\bar{1}0]$ direction, and (c) the intensity of the S_1 state is reduced by approximately one-half on the γ surface as compared to the α phase.

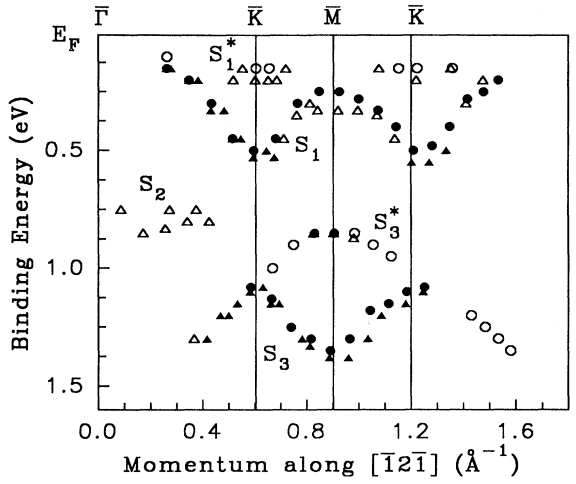

FIG. 6. The energy dispersion of the surface states detected for the α and γ phases along the $\bar{\Gamma}\bar{K}\bar{M}$ direction. The circles and triangles indicate results for the α and γ phases, respectively. Solid (open) symbols denote strong (weak) features in the photoemission spectra.

Most of the surface electronic structure displayed in Figs. 6 and 7 is known to arise from the adatom-substrate bonding interaction. Features similar to S_3 and S_3^* have been found on several metal/Si(111)-$(\sqrt{3}\times\sqrt{3})R30°$ systems, and are known to be due to the back bonds which comprise the T_4 adatom complex. As first shown in a theoretical study by Northup for the Al/Si(111)-$(\sqrt{3}\times\sqrt{3})R30°$ surface, these "back-bonding" surface bands arise from adatom p_x and p_y orbitals coupled to "dangling" substrate p_z orbitals.[5] In the present case the

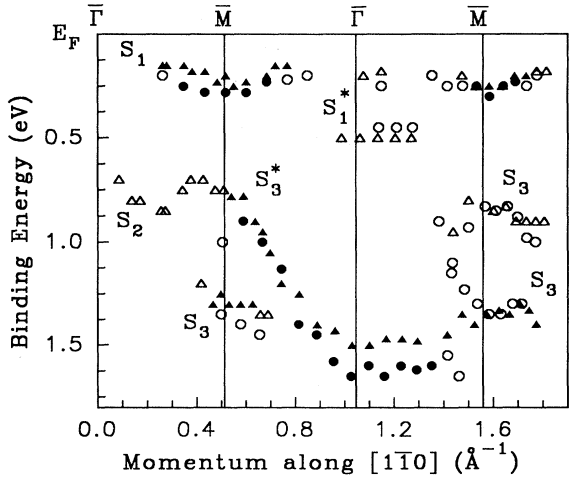

FIG. 7. Same as Fig. 6 except that the momentum varies along the $\bar{\Gamma}\bar{M}$ direction.

substrate is Ge(111) and the adatoms are neither Pb atoms only (for the α phase) or a combination of Pb and Ge adatoms (for the γ phase). This coupling gives rise to two surface states, labeled Σ_3 according to Northup's notation, ranging from 0.8 to 2 eV below the Fermi level, depending on the atomic species of the adsorbate/substrate.[6]

For group-IV adatoms (Si, Ge, Sn, Pb), an additional state has been observed in the 0–0.5-eV binding-energy range.[1,7,16] This surface state, being dispersive, shows a strong emission intensity, especially around the $\bar{K}$ points in the surface Brillouin zone. For the Pb/Si(111) (Ref. 16) and Sn/Si(111) (Ref. 1) systems, this S_1 state follows the periodicity of the $(\sqrt{3}\times\sqrt{3})R30°$ Brillouin zone, whereas for surfaces such as Si(111)-(7×7) (Refs. 4 and 7) and Ge(111)-c(2×8) (Refs. 17 and 18) it follows the bulk-terminated (1×1) periodicity. The atomic origin of this S_1 state is known to be due to adatom p_z orbitals coupled to substrate dangling bonds. In the case of group-III adsorbates, this band is above the Fermi level, whereas for group-IV adatoms this band should be half filled, ideally.[6] The model $(\sqrt{3}\times\sqrt{3})R30°$ group-IV-adatom reconstructed surface is thus *metallic*. This state, labeled Σ_1 according to Northup's notation, is often referred to as a dangling-bond state.

For group-III adatoms (Al,Ga,In), a state has been detected at about 0.3 eV below the Fermi level.[1] These S_1 surface states have very little dispersion and are usually weak structures. For some time it was believed that the origin of these surface states was due to domain boundaries.[1] STM study determined instead that the origin of these states is due to varying concentrations of Si adatoms on these surfaces in T_4 sites; i.e., due to the presence of mosaic phases.[12]

Figure 8 summarizes the dispersive behavior of the surface states, detected from the α and γ phases, in the reduced zone. This figure displays a partial set of data taken from Figs. 6 and 7, along the $\bar{\Gamma}\bar{K}\bar{M}$ and $\bar{M}\bar{\Gamma}$ segments, respectively. Also shown in this figure are some of the theoretical bands, as calculated by Northup *et al.*, for Si and Al adatoms.[5,6] The calculated adatom dangling-bond Σ_1 band [based on the Si/Si(111)-$(\sqrt{3}\times\sqrt{3})R30°$ system][6] and back-bonding Σ_3 bands [based on the Al/Si(111)-$(\sqrt{3}\times\sqrt{3})R30°$ system][5] are shown in Fig. 8 as solid lines. The theoretical studies have found that the energy position and bandwidth of the Σ_1 and Σ_3 bands vary with the type of adatom present, but that the general shape of the dispersions are qualitatively equivalent. The choice of theoretical data for the Σ_3 band yielded the closest qualitative agreement in energy position with our data. Clearly, the general shape of the predicted bands follows the experimental ones well. We note that the intensity dependence of the S_3 and S_3^* bands with $\mathbf{k}_\parallel$ is also consistent with theory.[2,5,6]

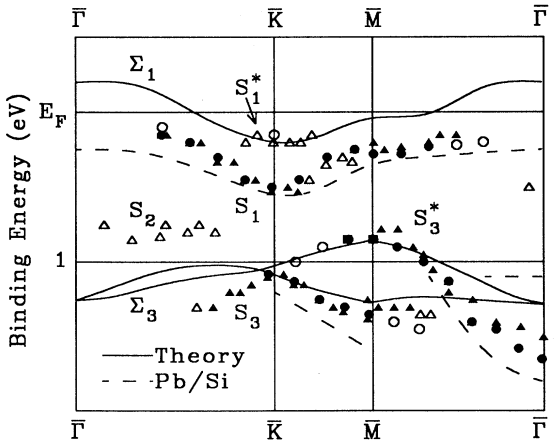

FIG. 8. A comparison of the experimental dispersions found in this work with theoretical ones as calculated in Refs. 5 and 6. The solid and open symbols represent part of the data taken from Figs. 6 and 7, whereas the solid lines are the calculated adatom dangling-bond (Σ_1) and back-bonding (Σ_3) surface bands (from Refs. 6 and 5, respectively). The dashed lines are the surface bands detected for the Pb/Si(111)-$(\sqrt{3}\times\sqrt{3})R30°$ mosaic (γ) phase from Ref. 16.

Another observation consistent with the theory is that these Pb/Ge(111) α and γ phases are *metallic*. As was observed by us previously in our angle-integrated study,[11] the density of states at the Fermi level is quite significant. It follows therefore that the S_1 band must cross the Fermi level. This Fermi-level crossing is discernible at several angles in Figs. 2–5. For example, the S_1 state appears to go below the Fermi level as the emission angle is varied from 5° to 7.5°. Based on our data and the information in Figs. 6–8, we deduce this Fermi-level crossing to be approximately $\frac{1}{3}$ of the way between the symmetry points along the $\bar{\Gamma}\bar{M}$ and $\bar{\Gamma}\bar{K}$ directions.

It is interesting to note that the submonolayer $(\sqrt{3}\times\sqrt{3})R30°$ phases of the Pb/Si(111) system, which are identical in structure and Pb coverage to the Pb/Ge(111) α and γ phases, are *semiconducting*. Our own angle-integrated valence-band data,[10] as well as a recent angle-resolved study by Karlsson *et al.*,[16] have indicated that each of these phases for Pb/Si(111) has a very small, if not zero, density of states at the Fermi level. The angle-resolved results for the Pb/Si(111) mosaic (γ) phase are summarized in Fig. 8 by the dashed lines. Note that the S_1 state is detected throughout the entire surface Brillouin zone in this study, and is clearly below the Fermi level. The S_3 and S_3^* states appear slightly shifted by 0.1 eV to lower binding energies for the Pb/Ge surface as compared to the Pb/Si system.

The theoretical work discussed above does not, however, predict the presence of two distinct states near the Fermi level. We therefore propose that the very weak S_1^* emission is derived from a density-of-states feature. This interpretation is consistent with the observations that S_1^* is detected on both the α and γ surfaces and is dispersionless within our experimental error. For data taken along $[\bar{1}2\bar{1}]$ and $[1\bar{1}0]$ (see Figs. 6 and 7), the S_1^* feature can be associated with the high density of states near $\bar{M}$ and $\bar{K}$, respectively. Note that the γ phase has a mosaic structure, and the mix of the Pb and Ge adatoms can give rise to scattering and mixing of different wave vectors of the adatom state. This explains the fact that, for the γ phase, the S_1^* feature is generally more pronounced, and the S_1 intensity is reduced, compared to the α phase.

As opposed to the S_1 (S_1^*) states, the S_3 and S_3^* states are very similar for the two phases. Along the $[\bar{1}2\bar{1}]$ direction, these bands for the two phases simply overlapped each other. A shift of approximately 0.15 eV was detected along the $[1\bar{1}0]$ direction near the second $\bar{\Gamma}$ point. The fact that these states have essentially the same intensity on both the α and γ surfaces indicates that the Pb and Ge back-bonding states are essentially equivalent.

The S_2 state cannot be accounted for based on previous work on adatom-induced surface electronic structure. The energy position of the S_2 state and the fact that it is only detectable over a small portion of the surface Brillouin zone may indicate that it is the result of vacancy defects. Areas where the T_4 sites are not occupied by Pb or Ge adatoms would give rise to one substrate dangling bond in the first layer per $(\sqrt{3}\times\sqrt{3})R30°$ unit cell. These "rest-atom" dangling p_z bonds could give rise to surface states similar to rest-atom states found on the Si(111)-(7×7) (Refs. 4 and 7) and Ge(111)-c(2×8) (Refs. 17 and 18) reconstructed surfaces. We note that the S_2 state found in a recent angle-resolved study of the Pb/Si(111) mosaic phase may be accounted for by these vacancy defects as well.[16]

V. SUMMARY

The Pb/Ge(111) system has been probed with angle-resolved photoemission spectroscopy. The $E_b(\mathbf{k}_\parallel)$ dependence of the adatom-induced surface states on the α and γ reconstructed surfaces have been mapped out along the $[\bar{1}2\bar{1}]$ and $[1\bar{1}0]$ directions. For the α phase, the electronic structure follows what has been predicted and observed in several prototypical metal/Si(111) systems. The dispersions of the adatom-induced back-bonding surface states follow both the general shape and intensity variations as predicted by Northup for T_4 complexes.[5,6] Our results indicate that, despite their structural differences, the α and γ phases have essentially the same electronic structure. The differing dangling-bond states are essentially equivalent on the two surfaces. The only difference is a slight shift for the S_3 (S_3^*) band over a small portion of the surface Brillouin zone.

ACKNOWLEDGMENTS

This work was supported by the U.S. Department of Energy (Division of Materials Sciences, Office of Basic Energy Sciences) under Grant No. DEFG02-91ER 45439. We acknowledge the Donors of the Petroleum Research Fund, administered by the American Chemical Society, and the U.S. National Science Foundation (Grant No. DMR-89-19056) for partial personnel and/or equipment support. We acknowledge the use of central facilities of the Materials Research Laboratory of the University of Illinois. The Synchrotron Radiation Center of the University of Wisconsin–Madison is supported by the U.S. National Science Foundation.

[1]T. Kinoshita, S. Kono, and T. Sagawa, Phys. Rev. B **34**, 3011 (1986).
[2]J. M. Nicholls, P. Mårtensson, G. V. Hansson, and J. E. Northup, Phys. Rev. B **32**, 1333 (1985).
[3]R. I. G. Uhrberg, G. V. Hansson, J. M. Nicholls, P. E. S. Persson, and S. A. Flodström, Phys. Rev. B **31**, 3805 (1988).
[4]T. Kinoshita, S. Kono, and T. Sagawa, Phys. Rev. B **32**, 2714 (1985).
[5]J. E. Northup, Phys. Rev. Lett. **53**, 683 (1984).
[6]J. E. Northup, Phys. Rev. Lett. **57**, 154 (1986).
[7]P. Mårtensson, A. Cricenti, L. S. O. Johansson, and G. V. Hansson, Phys. Rev. B **34**, 3015 (1986).
[8]B. P. Tonner, H. Li, M. J. Robreht, M. Onellion, and J. L. Erskine, Phys. Rev. B **36**, 989 (1987).
[9]R. P. Elliott, *Constitution of Binary Alloys, Supplement 1* (McGraw-Hill, New York, 1965).
[10]J. A. Carlisle, T. Miller, and T.-C. Chiang, Phys. Rev. B **45**, 3400 (1992).
[11]J. A. Carlisle, T. Miller, and T.-C. Chiang, Phys. Rev. B **47**, 3790 (1993).
[12]R. J. Hamers and J. E. Demuth, Phys. Rev. Lett. **60**, 2527 (1988).
[13]E. Ganz, F. Xiong, Ing-Shouh Hwang, and J. Golovchenko, Phys. Rev. B **43**, 7316 (1991).
[14]W. D. Grobman, D. E. Eastman, and J. L. Freeouf, Phys. Rev. B **12**, 4405 (1975).
[15]T.-C. Chiang, J. A. Knapp, M. Aono, and D. E. Eastman, Phys. Rev. B **21**, 3513 (1980).
[16]C. J. Karlsson, E. Landemark, Y.-C. Chao, and R. I. G. Uhrberg, Phys. Rev. B **45**, 6321 (1992).
[17]J. M. Nicholls, G. V. Hansson, and R. I. G. Uhrberg, Phys. Rev. B **33**, 5555 (1986).
[18]J. Aarts, A. J. Hoeven, and P. K. Larson, Phys. Rev. B **37**, 8190 (1988).